Desalination and Water Treatment
www.deswater.com

doi: 10.5004/dwt.2020.26292

204 (2020) 114–123
November

Effective and selective removal of anionic dye-based on wasted magnetic chitosan immobilized cellulase beads

Lei Hu[a,†], Chao Yang[a,†], Limin Zang[a,*], Qifan Liu[b], Jianhui Qiu[b], Jun Yang[a], Xuan Qiao[a], Xue Yang[c,*], Huihao Li[a]

[a]*Key Laboratory of New Processing Technology for Nonferrous Metal and Materials (Ministry of Education), and College of Materials Science and Engineering, Guilin University of Technology, Guilin 541004, China, Tel. +86 773 5896672; emails: 2016034@glut.edu.cn (L.M. Zang), hlpolymer010@gmail.com (L. Hu), yangchao_chem@163.com (C. Yang), yjun013@gmail.com (J. Yang), qiaoxuan150103@gmail.com (X. Qiao), l442068663@gmail.com (H.H. Li)*

[b]*Department of Machine Intelligence and Systems Engineering, Faculty of Systems Science and Technology, Akita Prefectural University, Yurihonjo 015-0055, Japan, Tel. +81 184 272134; emails: liuqifan0108@gmail.com (Q.F. Liu), qiu@akita-pu.ac.jp (J.H. Qiu)*

[c]*Department of Anesthesiology, Huashan Hospital, Fudan University, Shanghai 200040, China, Tel. +81 2152887694; email: yangxue5611@126.com (X. Yang)*

Received 1 July 2019; Accepted 27 June 2020

ABSTRACT

The removal of dyes from wastewater by wastes has already attracted a great deal of attention for being in line with the idea of "treating the wastes with wastes". In this study, the waste chitosan magnetic beads immobilized cellulase (CMP-IC) was applied in the adsorption of Orange G (OG) anionic dyes, so as to investigate the kinetics, isotherm and thermodynamics of the adsorption process. Providing porous structures and specific surface areas for OG molecules, CMP-IC possessed a higher adsorption rate at pH = 4 and suited with pseudo-second-order kinetic belong to rate-limiting step. Meanwhile, the adsorption was a spontaneous procedure that met the Langmuir isotherm described as monolayer adsorption. CMP-IC was selective in adsorbing OG anionic dye from the mixed dyes solutions and was efficient in reabsorbing OG for 5 cycles due to the excellent chemical and structural stabilities. Our study can provide new insights into utilizing waste materials for water treatment for various promising applications.

Keywords: Inactive enzyme; Selective adsorbent; Anionic dye; Magnetic separation; Reutilization

1. Introduction

The removal of dyes from wastewater is of practical significance, especially for reducing the environmental pollution. A variety of dyes are difficult to degrade due to their stability and oxidative resistance in the water environment. Besides, the toxicity and carcinogenic characteristics of dyes make them detrimental to the safety of biological organisms and humans [1–3]. Orange G (OG), is one of the anionic dyes with a mono azo structure that has been widely used in food colorant, leather products, printing and textile industry [4,5]. However, it presents a severe threat to the environment and the health of people due to its non-biodegradable nature, chronic toxicity and resistance to light irradiation [6]. In consideration of this, there is an absolute necessity to remove it from dyeing wastewater by means of water treatment.

* Corresponding authors.

† These authors contributed equally in this work.

Adsorption is regarded as an economically affordable and eco-friendly technique for the removal of dyes due to its high efficiency, excellent selectivity, recyclability and low cost [7–10]. In general, porous materials possess high uptake capacity and desirable kinetics interact with dyes molecule through a chemical or physical process, for which they are preferred as adsorbent [11]. In this regard, the appropriate selection of materials as adsorbent plays a vital role in achieving outstanding outcomes of adsorption.

It is inevitable for such conventional adsorbent as activated carbon, activating oxide or bio-adsorbent to incur a substantial amount of cost for water treatment [12–14]. Therefore, the porous waste produced by a lab study has attracted our attention. Not only does the application of them as adsorbent achieve the purpose of recycling, but it also makes them selective in the removal of dyes from wastewater, thus achieving the sustainable utilization of resources. Inspired by this, the wasted chitosan magnetic particle immobilized cellulase (CMP-IC) was taken as an effective and selective adsorbent of the OG aqueous solution. Among them, CMP-IC provides porous structures for OG molecule while the OG is treated as a model adsorbate to investigate the adsorption mechanism, kinetics and thermodynamics. OG is a typical type of anionic dye, for which the removal of it could lay a theoretical foundation for anionic dyeing water treatment in practice and further provide a low-cost method to get rid of toxic features dyes.

Yet most research on the treatment of printing and dyeing wastewater focus on the synthesized adsorbents or modified natural adsorbent. With the development of the industrial enzyme applications, how to dispose and recycle the spent enzyme catalyst becomes a noticeable problem. This study proposes a novel approach to recycling the wasted resources while realizing an efficient treatment of dyeing water. Use of the waste chitosan magnetic beads immobilized cellulase as adsorbents directly exhibited relatively higher adsorption ability and selective adsorption ability in dyes removal. For dyes adsorption, the amine groups on CMP-IC react with anionic dyes selectively, which is conducive to the separation of mixture wastewater. The structural diagram is shown in Fig. 1.

2. Materials and methods

2.1. Materials

Orange G, methylene blue (MB), hydrochloric acid (HCl) and sodium hydroxide (NaOH) were purchased from Aladdin Reagent Co., Ltd. (Shanghai, China). Distilled water was taken as a solvent in the experiments.

2.2. Preparation of adsorbent

The adsorbent of wasted CMP-IC was obtained from our previous work [15]. CMP beads were the first to be prepared. The entire process is detailed as follows. 4.0 g chitosan was added into 100 mL 2% acetic acid aqueous solution for complete dissolution with stirring. Subsequently, 16.0 g MP (magnetic particle) was uniformly dispersed in the above-mentioned chitosan solution to obtain CMP gel by continuous stirring for 1 h. Then, the gel mixture was instilled into a 50 mL kerosene oil phase containing 0.5 g Span-80 and 0.15 g Tween-80 and was stirred with 600 rpm for 2.5 h to obtain CMP gel spherical beads. Finally, the as-prepared beads were placed in a coagulation bath (80 mL of 2 M NaOH solution and 40 mL of ethyl alcohol) for 12 h before being separated magnetically and washed with distilled water for several times to prepare the CMP beads.

The as-prepared CMP beads reacted with 120 mL 2.5% glutaraldehyde aqueous solution for 2 h, before being repeatedly washed with distilled water after magnetic separation. Then, the glutaraldehyde activated CMP beads were mixed with 100 mL cellulase solution (6 mg/mL, 0.1 M acetate buffer as solvent) for 2 h of sufficient reaction assisted by stirring at ambient temperature. Finally, the CMP-IC was obtained by washing the immobilized cellulase with 0.1 M acetate buffer for several times and denoted as CMP-IC. In this study, CMP-IC as the adsorbent was collected when it lost the capability of biological activity after repeating hydrolyzes cellulose. Eventually, the CMP-IC was washed several times with distilled water and then refrigerated at 4°C.

2.3. Adsorption studies

The OG solution was prepared by dissolving OG powder in distilled water to reach different initial concentrations ranging from 120 to 270 mg/L. NaOH or HCl aqueous solution was used to adjust the pH of the OG solution within the range from 3 to 6. In the process of adsorption, 0.2 g CMP-IC has been added into a 50 mL OG solution by vibration in a thermostatic oscillator (150 r/min). After the elapse of a specified period of time, the adsorbent was separated by going through a magnetic separation process and the absorbance of the supernatant was tested using a UV-vis spectrophotometer (λ_{max} = 475 nm). The kinetics analysis of adsorption required

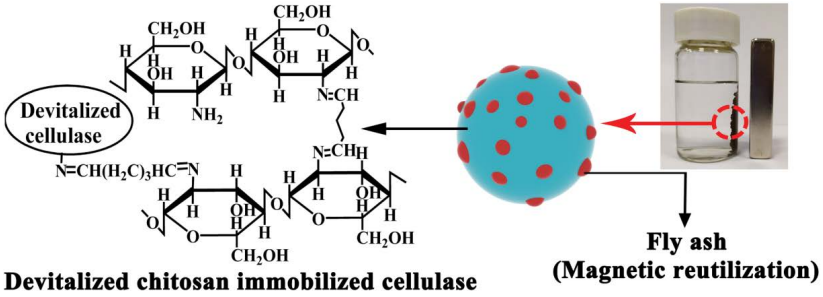

Fig. 1. Structure diagram of the devitalized chitosan magnetic particle immobilized cellulase.

varying contact times (0–1,440 min) with particular temperatures and pH values. The adsorption isotherms analysis was conducted to maintain the different initial concentrations of the OG solution for 24 h at 25°C. A selective adsorption study was performed by mixing OG (anionic dye, 180 mg/L) and MB (cationic dye, 180 mg/L) solution at pH = 4.

The adsorption capacity of CMP-IC was calculated using the following equation:

$$q_t = \frac{\left(C_0 - C_t\right) \times V}{m} \quad (1)$$

where q_t (mg/g) indicates the adsorption capacity; C_0 (mg/L) denotes the initial concentration of the OG solution, C_t (mg/L) refers to the concentration of OG solution at time t, V (L) stands for the volume of the OG solution and m (g) represents the mass of adsorbent.

2.4. Characterization

The Fourier-transform infrared spectroscopy (FTIR, Thermo Nicolet Nexus 470, USA) measurements were performed to determine the chemical structures in line with the KBr pellet method. Thermogravimetric analyzer (TGA, TA Instrument Q500, USA) was carried out and heated from 25°C to 800°C with a rate of 10°C/min under nitrogen atmosphere. The textural properties of CMP-IC were tested by an automatic specific surface and porosity analyzer (BELSORP-mini II, MicrotracBEL, Japan). The specific surface area was calculated via the Brunauer–Emmett–Teller (BET) method at 77 K, the relative pressure (P/P_0) ranged from 0 to 1. The morphology of the sample was characterized by field emission scanning electron microscope (SEM, HITACHI S-4800, Japan). The absorption wavelength of the OG solution was measured by the UV-vis spectrophotometer (UV-9000S, Shanghai Metash Instruments Co., Ltd., China). UV-vis absorption spectra of the absorbed solution were collected by a UV-vis spectrophotometer (752N, INESA Analytical Instrument Co., Ltd., China). The pH of the aqueous solution was tested using a pH meter (PHS-25, Shanghai Precision & Scientific Instrument Co., Ltd., China).

3. Results and discussion

3.1. Characterization of adsorbent

The FTIR spectroscopy of MP and CMP-IC are depicted in Fig. 2a; the corresponding various chemical structures of them are characterized. Obviously, the peak at 3,434 cm^{-1} revealed in both samples which belong to O–H and N–H stretching vibration. For CMP-IC, 2,929 and 2,859 cm^{-1} were ascribed to the stretching vibrations of the C–H bond. And then, the C=N vibrations of imines were incarnated at 1,631 cm^{-1} while the amide II was displayed in 1,569 cm^{-1}. It is worth noted that the unique peak at 1,410 cm^{-1} of CMP-IC primarily came from proteins, which demonstrated the cellulase was successfully immobilized on the CMP. In addition, the peaks around 1,068 and 557 cm^{-1} of MP were attributed to the asymmetric stretching vibrations of Si–O/Al–O and Fe–O bond, respectively [16].

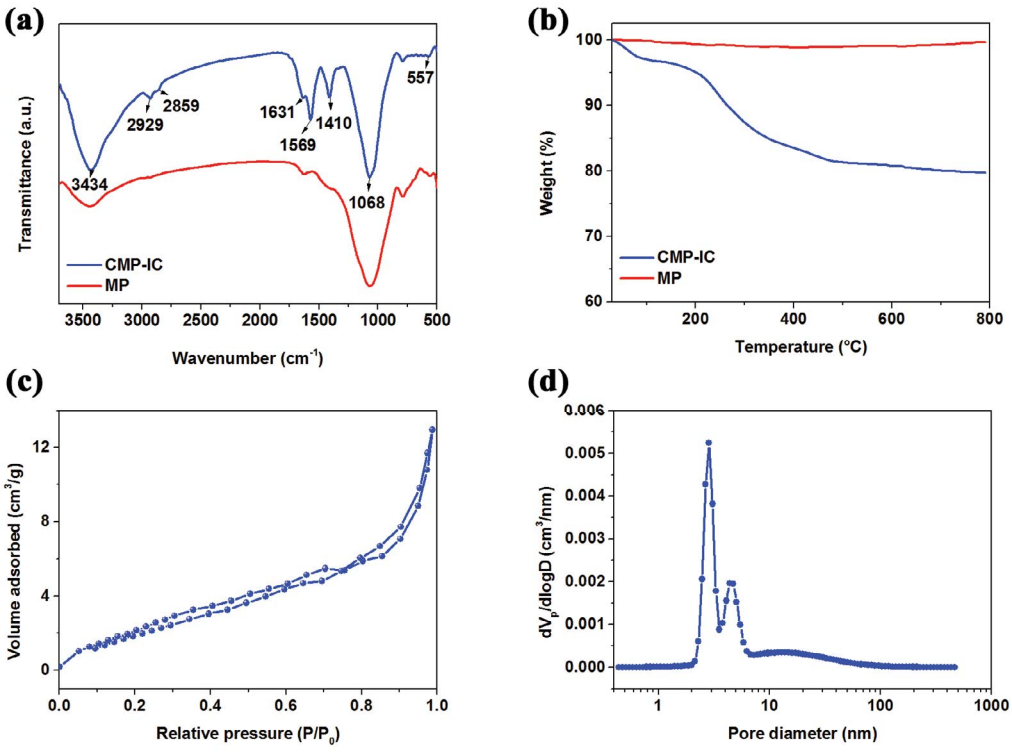

Fig. 2. (a) FTIR spectroscopy, (b) TGA curves of MP and CMP-IC, (c) N_2 adsorption–desorption curves of CMP-IC at 77 K, and (d) pore size distribution of CMP-IC.

Furthermore, the TGA curves of MP and CMP-IC are illustrated in Fig. 2b to assess thermal performance. The weight of MP was maintained without any significant decline even the temperature was raised to 800°C, indicating the extraordinary stability. CMP-IC exhibited weight loss at the first stage below 200°C, which was attributed to the water released in the structure and the surface of the polymer. Subsequently, the continuous process of heating caused the degradation of polysaccharide units, which led to the depolymerization of the chitosan chain revealed in the second stage [17,18]. Besides, the mass rate of chitosan and cellulose in the compound was estimated to be 20% at maximum according to the weight of the sample at 800°C. The result indicated that CMP-IC provided a mass of magnetic particles for the separation of adsorbent from the solution while continuing to offer the active substance of chitosan and cellulase for dyes adsorption.

The N_2 adsorption–desorption curve of CMP-IC is illustrated in Fig. 2c while the textural information is presented in Table 1. According to the IUPAC (International Union of Pure and Applied Chemistry) classification [19,20], the curve is classified into a typical IV-type sorption isotherm, indicating that CMP-IC exhibits abundant micropores and mesopores [9]. The BET specific surface area (S_{BET}) and total pore volume of CMP-IC are 10.523 (m^2/g) and 0.020 (cm^3/g), respectively. The pore size distribution (Fig. 2d) evidences that the pore size ranges primarily from 2 to 7 nm meanwhile possessed part mesopores. The mean pore diameter is shown to be 7.616 nm (Table 1), which offers a high capacity for dye molecules inside the pore structure.

The SEM images are introduced to facilitate investigation into the surface morphology of MP, and the changes are contributed to by the chitosan and immobilization process of cellulose. As shown in Fig. 3a, most sphere magnetic particles are normally 1 to 20 μm across. Furthermore, the MP possesses a rough surface that provides wide-area active sites for adsorption of dyes molecules in Fig. 3b. Moreover, the magnetic microspheres contribute to the fast separation of the MP compound in the experimental process. In contrast with MP, CMP-IC (Fig. 3c) exhibits larger multi-time beads after coating chitosan and the subsequent immobilization process. Apparently, the surface of CMP-IC has been filled with cellulase and tiny particles fully (Fig. 3d), while the high magnification view demonstrated the porous structure (inset view) provides sites for absorption of dye molecules. The amino groups of cellulase are introduced to react with

Table 1
Textural properties of CMP-IC

V_m (cm^3(STP)/g))	S_{BET} (m^2/g)	Total pore volume (cm^3/g)	Mean pore diameter (nm)
2.418	10.523	0.020	7.616

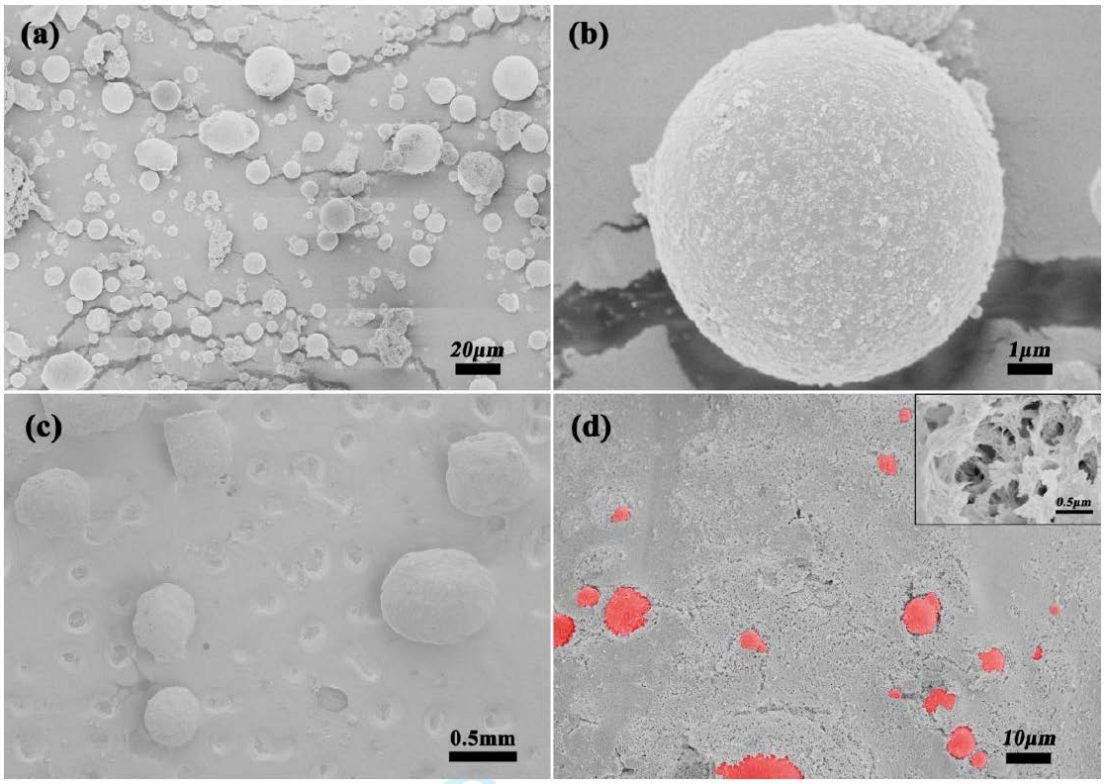

Fig. 3. SEM images of the surface of MP (a and b) and CMP-IC (c and d).

the aldehyde groups of coupling agents of glutaraldehyde that has activated the primary amino groups of microspheres, for subsequent covalent linkage to immobilize cellulase onto CMP [21].

3.2. Effect of pH and contact times

The pH value of the solution is one of the most significant factors in the evaluation of adsorption property throughout the process, especially for the ion exchange and electrostatic interaction process [22]. In general, the values of pH tend to exert influence on not only the functional groups of the adsorbent but also the charges of the adsorbate [23]. In this section, the OG molecule (Fig. 4a) gives rise to two sulphonate groups and one hydroxyl group that characterizes the nature of anionic in aqueous solution, which implies the multiple states (Fig. 4b) at different pH values. As shown in Fig. 4c, the adsorption rate of the adsorbent is increased rapidly with the pH value increased but decreased later. The highest adsorption rate is 92.6% at pH = 4, and each adsorption rate is in excess of 80%. The changes in the adsorption rate are attributed to the change of the molecular state in the medium. OG maintains the molecular state (Fig. 4b left) at the lower pH of a solution, which is conducive to adsorption due to the hydrophobic acid-base interaction. The continuous increase of pH value causes the property of adsorption to deteriorate. This is due to the change of the ionic state (Fig. 4b right) of OG. This phenomenon is primarily ascribed to the improved hydrophilicity and solubility of adsorbate after the ionization of OG, it results in a decline of adsorption rate [6]. Additionally, the increased pH value of aqueous solution could even indicate the generation of more anions. Therefore, it is speculated that the behavior of anionic electrostatic repulsion is another reason for the deteriorating adsorption performance with the increase of pH value [22]. In this case, pH = 4 is treated as the optimal value of the medium to perform the adsorption study.

The adsorption capacity of CMP-IC onto OG at different contact times is indicated in Fig. 4d. Apparently, the capacity increases rapidly during the first 120 min. Then, it continued to increase but at a slow pace until the time point of 480 min, before ending up being steady at the time point of 1,440 min. This is attributed to the massive active adsorption sites on the surface of CMP-IC, which results in a fast rate of adsorption in the first stage. Continuously, the OG molecules require a long path and more time to arrive at the inner pores with the decline of dye concentration in solution in the second stage [24]. The further adsorption process causes pores of CMP-IC to be fully filled until the equilibrium is reached which possesses a constant adsorption capacity even in overtime. As evidenced by the result, the numerous pores uniformly distributed in CMP-IC are particularly conducive to the transfer of dye molecules while ensuring a high absorption efficiency. Moreover, OG initial concentrations led to different effects on capacity throughout the period, while the higher concentration contributed to a larger amount of adsorption. This is because the concentration gradient accelerated the diffusion of OG molecule from

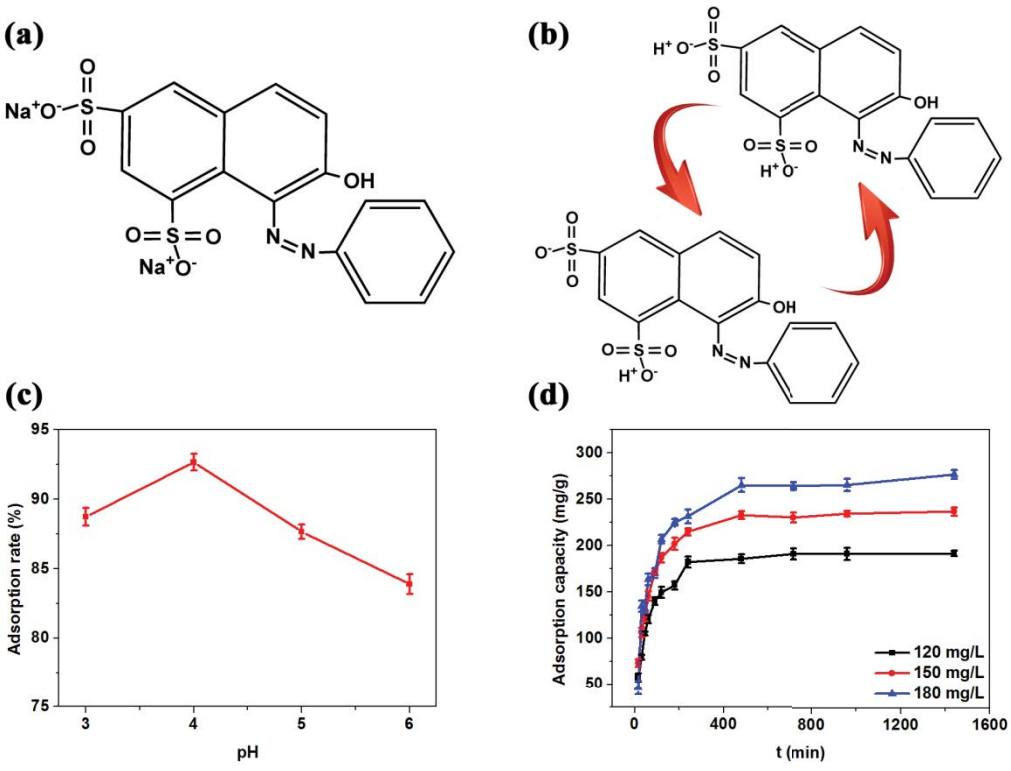

Fig. 4. (a) Molecule structure of OG, (b) transformation of the OG molecule states, (c) adsorption rate at different pH (C_0 = 180 mg/L; t = 1,440 min; T = 298 K), and (d) effect of contact times on OG (T = 298 K; pH = 4; 150 r/min; λ_{max} = 475 nm).

solution to CMP-IC, thus improving the capacity of absorption. Meanwhile, the correlation between capacity and time is worth to address the mechanism of adsorption issue. The results possess guiding significance and reference value to the practice for treating industry acidic wastewater.

3.3. Adsorption kinetics and isotherms analysis

Generally speaking, the mechanisms of adsorption involve physical and chemical procedures, ion exchange and chelation [22]. Therefore, two adsorption kinetic models are applied to describe the transfer of dye molecules onto the adsorbent of CMP-IC particles, and a suitable model is taken as reference for practical operations. The homologous two linear models equations are expressed as follows [25,26]:

Pseudo-first-order kinetic model:

$$\ln\left(q_e - q_t\right) = \ln q_e - k_1 t \tag{2}$$

Pseudo-second-order kinetic model:

$$\frac{t}{q_t} = \frac{t}{q_e} + \frac{1}{k_2 q_e^2} \tag{3}$$

where q_t (mg/g) represents the adsorption capacity at time t, q_e (mg/g) indicates the adsorption capacity at equilibrium state, k_1 (1/min) and k_2 (g/(mg min)) denotes the rate constant of the pseudo-first-order kinetic and pseudo-second-order kinetic, respectively.

Figs. 5a and b present the fitted curves of pseudo-first-order and pseudo-second-order model, while the kinetic parameters are listed in Table 2. The correlation coefficients (R^2) of linear fitted from data is significant for the selection of the kinetic model to analyze the mechanisms of OG adsorbed onto CMP-IC. As shown in Table 2, the values of R^2 of pseudo-second-order fitted curves are higher than 0.999 and larger than pseudo-first-order parameters. Especially, the $q_{e,\text{cal.}}$ (calculate) of every concentration is closer to $q_{e,\text{exp.}}$ (experimental), indicating that the pseudo-second-order kinetic model is suited to this adsorption process. Based on the results as mentioned above, the adsorption system of OG onto CMP-IC is primarily classed into the rate-limiting step which stemmed from chemical adsorption with ion exchange [26,27].

For further quantification of the adsorption capacity and understanding of the interaction between OG and CMP-IC, the model known as "adsorption isotherm regional analysis model" (ARIAN model) is applied to conduct isotherms analysis. According to the literature, the ARIAN model can be split into four regions, which could be interpreted by different adsorption isotherms [28]. Region 1 implies that adsorption increases linearly, as revealed usually in the low adsorbate concentrations. Region 2 starts with the hemimicelle concentration, which is studied by an appropriate isotherm such as Temkin or Langmuir isotherms and represents only monolayer surface aggregate forms. As for region 3, it is characterized by bilayer adsorption isotherm equation when the new surface clusters and aggregates are shaped. In respect of the adsorption process, it is derived from the formation of a monolayer and can be fitted by applying the Langmuir-type equation. Region 4 emerges as a maximum adsorption capacity and is treated as a plateau or decreasing curve [29–31]. In this part, region 1 and region 4 are nonexistent as observed so that there are just region 2 and region 3 (Fig. 5c). It indicates that the adsorption is possible to occur on the two different sites. To further prove the adsorption interaction between OG and CMP-IC in region 2 and region 3, three isotherm models including Langmuir, Freundlich and Temkin are presented as follows [25,32,33]:

Langmuir model:

$$\frac{C_e}{q_e} = \frac{C_e}{q_m} + \frac{1}{q_m K_L} \tag{4}$$

Freundlich model:

$$\ln q_e = \frac{1}{n}\ln C_e + \ln K_F \tag{5}$$

Temkin isotherm model:

$$q_e = A + B \ln C_e \tag{6}$$

where C_e (mg/L) indicates the concentration of dye at equilibrium, q_e (mg/g) denotes the adsorption quantity at equilibrium, and q_m (mg/g) represents the maximum adsorption quantity in this system. K_L and K_F refer to the adsorption constants of the Langmuir and Freundlich models, respectively. The parameter of $1/n$ is defined as the adsorption intensity constant of the adsorbent. A and B denote the Temkin constants.

As mentioned before, the Langmuir model is one of the most-used isotherm models which rest on the assumption that monolayer adsorption possesses adsorption sites and energy distributed uniformly. The Freundlich model is suited to the heterogeneous surfaces and represents multilayer adsorption. Temkin isotherm model has described the effects of adsorbate–adsorbent interactions which are used widely in the investigation of adsorption [34]. Fig. 5d–f presents three models of linear fitted curves, the corresponding parameters listed in Table 3. Evidently, the R^2 values of the Langmuir model are in excess of 0.99 and higher than Freundlich and Temkin isotherms models, suggesting that the Langmuir model is more applicable to this adsorption equilibrium process. According to the Langmuir isotherm model, the adsorption mechanism is possibly described as monolayer adsorption and uniform activity distribution instead of a heterogeneous process, and the maximum amount of adsorption reaches 101.5 mg/g. Therefore, it can be inferred that region 2 and region 3 conform only to the monolayer adsorption. The results demonstrated that the behavior of OG onto CMP-IC is consistent with the chemical monolayer adsorption procedure as mentioned before.

3.4. Thermodynamic analysis

To achieve the effects of temperature during the adsorption process, such thermodynamic parameters as enthalpy change (ΔH), entropy change (ΔS) and Gibbs free energy change (ΔG) are investigated by fitted data at different

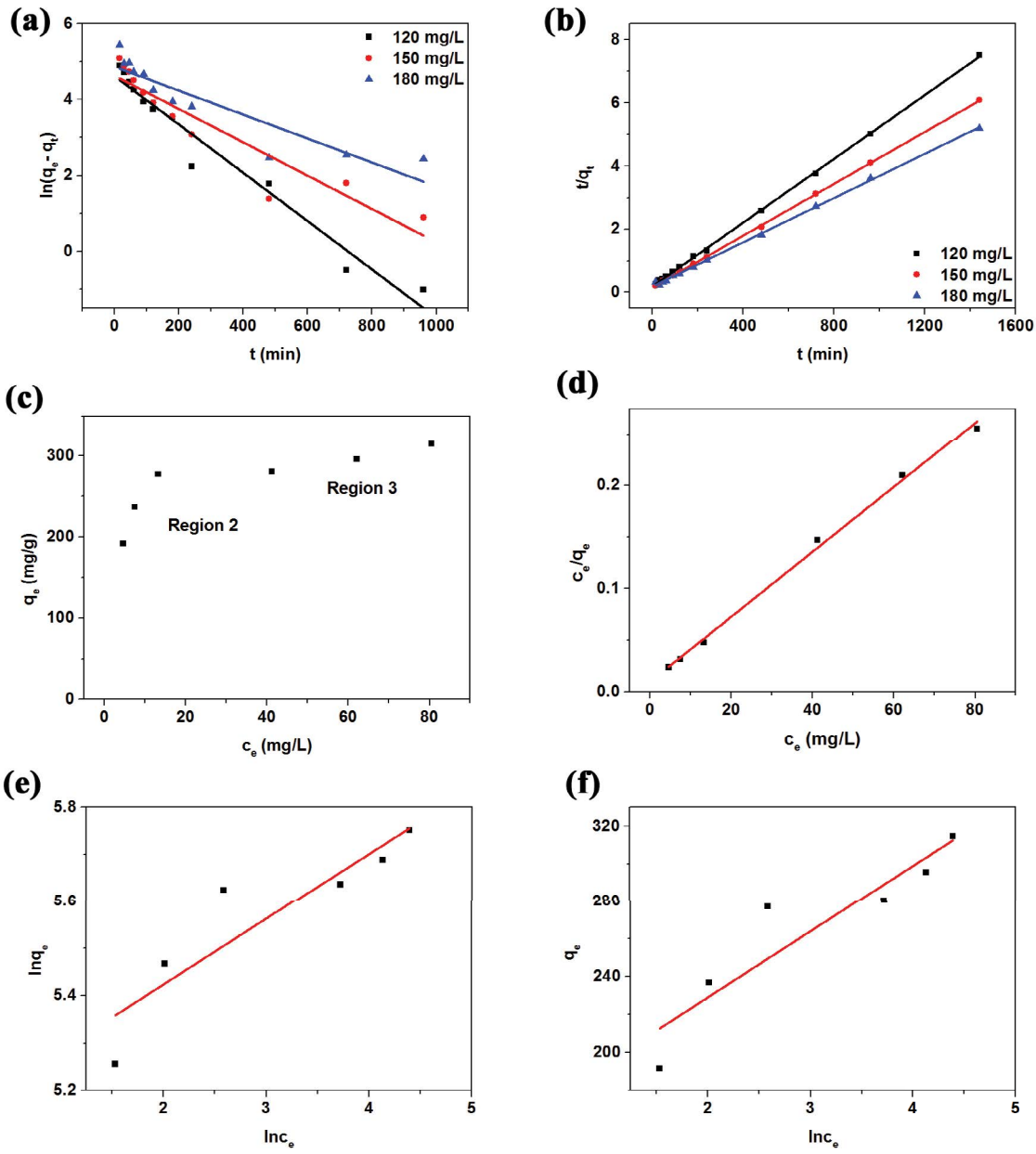

Fig. 5. (a) Pseudo-first-order adsorption kinetic fitted curve, (b) pseudo-second-order adsorption kinetic fitted curve, (c) adsorption isotherm according to the ARIAN model, (d) Langmuir model fitted curve, (e) Freundlich model fitted curve, and (f) Temkin model fitted curve.

Table 2
Kinetic parameters of first-order and second-order adsorption kinetic linear models

Models		Pseudo-first-order kinetic model			Pseudo-second-order kinetic model		
OG (mg/L)	$q_{e,exp.}$ (mg/g)	k_1 (1/min)	$q_{e,cal.}$ (mg/g)	R^2	$k_2 \times 10^{-3}$ (g/(mg min))	$q_{e,cal.}$ (mg/g)	R^2
120	191.6	0.00637	101.723	0.9588	0.1368	198.0	0.9996
150	236.7	0.00439	102.810	0.8725	0.1121	243.3	0.9998
180	277.0	0.00316	130.075	0.8214	0.0672	284.9	0.9999

Table 3
Parameters of adsorption isotherm models of OG absorption onto CMP-IC

Models	Langmuir model		Freundlich model			Temkin model		
Parameters	q_m (mg/g)	K_L (L/mg)	R^2	K_F (mg/g)	1/n	R^2	A	B	R^2
	101.52	3.137	0.996	171.46	0.139	0.785	158.94	34.99	0.824

reaction temperatures (298, 308 and 318 K). The values of ΔH and ΔS are calculated by applying the Van't Hoff equation, and the ΔG is presented as follows [24,35]:

$$\ln\left(\frac{q_e}{c_e}\right) = -\frac{\Delta H}{RT} + \frac{\Delta S}{R} \tag{7}$$

$$\Delta G = \Delta H - T\Delta S \tag{8}$$

where q_e (mg/g) and C_e (mg/L) represent the adsorption capacity and concentration at equilibrium, respectively. T (K) indicates the temperature in experimental adsorption. R stands for the universal gas constant 8.314 J/mol K. The enthalpy (ΔH) and entropy (ΔS) are obtained by calculating the slope and intercept.

The thermodynamic fitted curve and parameters are presented in Fig. 6 and Table 4, respectively. As revealed by the calculation results, all the values are negative, of which the ΔH is lower than 0, indicating the adsorption issue is an exothermal process. With regard to ΔG, the negative values indicated that the adsorption behavior belongs to the spontaneous procedure and that increasing the reaction temperature is contradictory to the progress of adsorption reaction. A smaller amount of ΔS suggests an insignificant change in entropy.

Table 4
Thermodynamic parameters of OG onto CMP-IC

T (K)	ΔG (kJ/mol)
298	–1.206
308	–1.044
318	–0.881
ΔH (kJ/mol)	–6.042
ΔS (kJ/mol K)	–0.0162

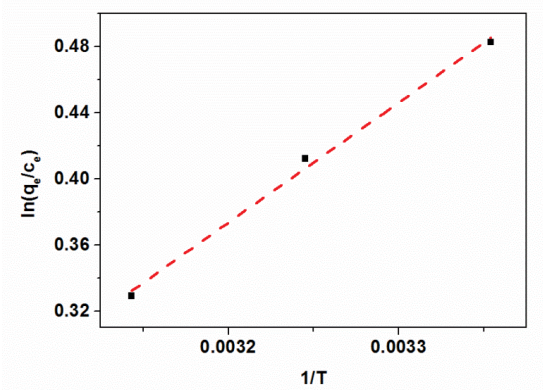

Fig. 6. Thermodynamic fitted curve of OG onto CMP-IC (C_0 = 180 mg/L; t = 1,440 min; pH = 4; 150 r/min).

3.5. Selective adsorption and reusability study

The adsorbent selectively adsorbed from mixed dyes is useful for practical application. As a kind of commonly-used anionic dyes, OG has been widely applied as an acid-base indicator and colorant by virtue of sulfonate and hydroxyl groups of the molecule. In an acid medium, a large number of hydrogen ions facilitated the reaction of sulfonic acid with amine groups on the CMP-IC, thus accelerating the process of adsorption. By contrast, the same phenomenon is not existent for cationic dyes (such as MB). Therefore, CMP-IC is taken as a selective adsorbent to remove anionic dyes from a mixed solution in acid medium. Fig. 7a presents the MB solution (1), OG solution (3) and the mixture of MB and OG (2) while the UV-vis spectra of the mixture are illustrated in Fig. 7b. According to the UV-vis spectra, the characteristic peak of OG at 475 nm vanishes after adsorption from the mixture solutions, which indicates that CMP-IC is highly efficient in the selective adsorption of anionic dyes. The effect of selective adsorption is illustrated in Fig. 7b (inset image).

The reusability of adsorbent has attracted much attention for practical significance, increase not only the repeating utilization factor of adsorbent but also decrease the wasting of resources. In this section, CMP-IC is separated and washed several times with 1 M KCl aqueous solution after the absorption of OG molecules. Then, desorption using HCl solution with pH = 4. Subsequently, the treated CMP-IC as an adsorbent for dye solution cycled five times, with the results shown in Fig. 7c. With the increase in the number of cycles, the removal efficiency exhibits a downward trend. A rate of approximately 69% is maintained even after the number of cycles reached five, which is primarily attributed to the interconnection pore structure (shown in SEM images) that provided plenty of adsorption sites to facilitate dyes transfer after adsorption/desorption cycles [36]. Furthermore, CMP-IC is characterized after 5 adsorption cycles, as shown in Figs. 7d–f. The FTIR of CMP-IC exhibits almost unaltered chemical structures, implying excellent chemical durability during several cycles. Moreover, the corresponding SEM images of CMP-IC are presented in Figs. 7e and f. It can be observed that the magnetic microsphere is preserved completely without break, and a large amount of MP remains embedded in the microsphere securely. Meanwhile, the porous structures (insert image in Fig. 7f) are found interconnected to maintain stability, which is contributed to the outstanding

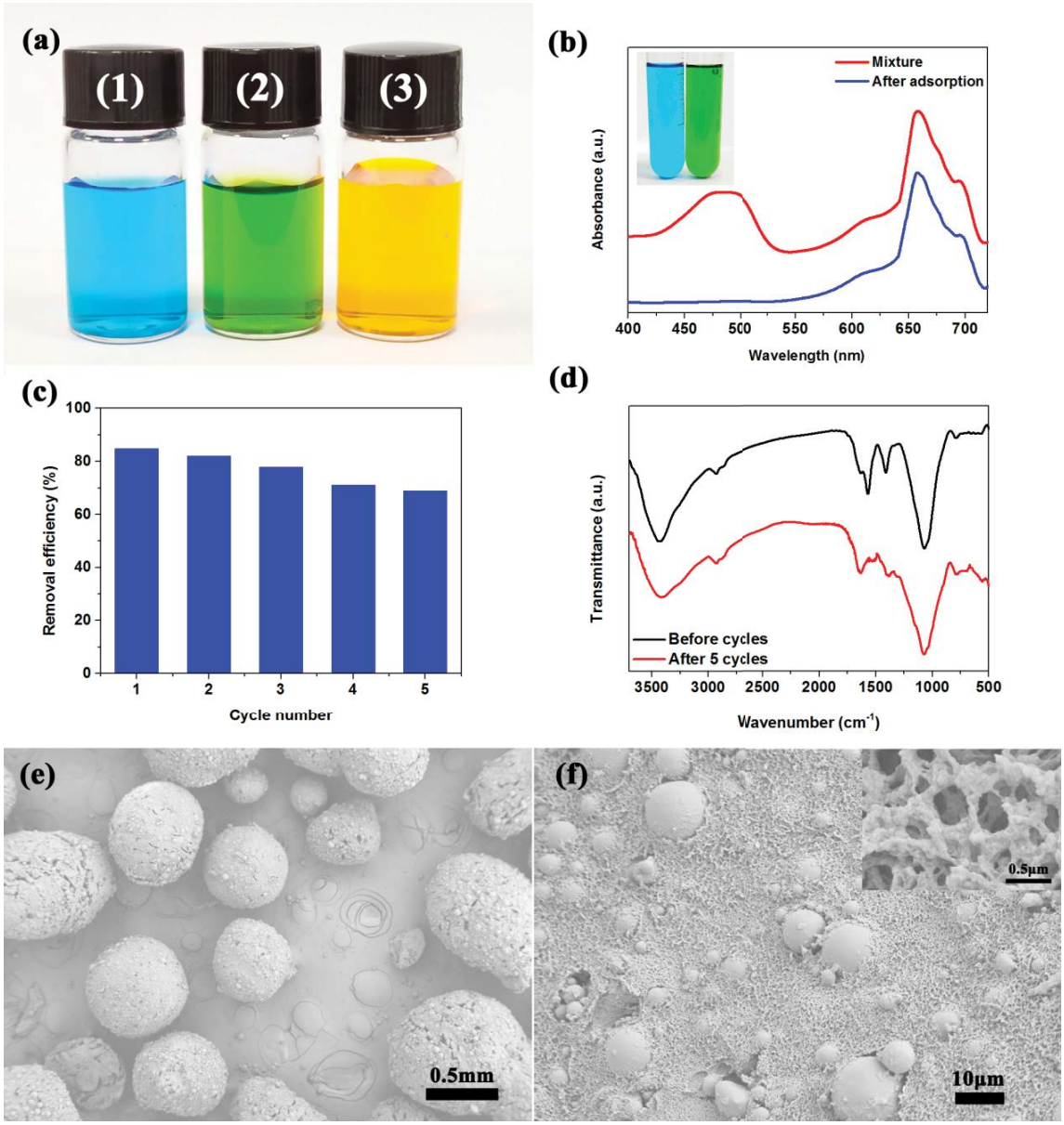

Fig. 7. (a) Digital photographs of MB (1), OG (3) and their mixture (2), (b) UV-vis spectra of the mixture adsorption (C_0 = 180 mg/L; T = 298 K), (c) reusability study of CMP-IC (C_0 = 180 mg/L; t = 1,440 min; pH = 4; 150 r/min), (d) FTIR curve of CMP-IC after 5 cycles. SEM images of CMP-IC microsphere (e), CMP-IC surface, and (f) and the porous structure (insert image).

adsorption capacitance for CMP-IC. This is identified with before mentioned pore features, indicating that the CMP-IC possesses excellent structural stability even after the repeated adsorption-desorption process. Based on the results as mentioned above, CMP-IC demonstrates excellent performances in the reutilization of adsorbing dyes, which provides a novel approach to achieving both high efficiency and selective adsorption from dyestuffs mixture.

4. Conclusion

In summary, we proposed a novel approach to treat the OG molecule with waste CMP-IC as an effective and selective adsorbent, accomplished with satisfactory outcomes and sustainable utilization of resources. Plenty of stable micropores and mesopores of CMP-IC provide enormous volumes for dye molecules, possessed the maximum adsorption of 101.5 mg/g with pH = 4. The adsorption procedure vested in a rate-limiting step that stemmed from chemical adsorption with ion exchange, while the ARIAN model verified that the process belongs to monolayer adsorption behavior. Moreover, the adsorption process was spontaneous and selective that proton promoted CMP-IC to interact with sulphonate and hydroxyl groups on OG. According to FTIR and SEM measurements, CMP-IC exhibited not only excellent chemical and structural stabilities but also outstanding adsorption sustainability and selective absorbability, which was better than previously reported adsorbent. The wasted

CMP-IC was expected to be an ideal effective and selective adsorbent, it provides new insights into utilizing waste materials in the field of water treatment.

Acknowledgments

The work was supported by the Guangxi Natural Science Foundation (No. 2017GXNSFBA198085), Scientific Research Foundation of the Guilin University of Technology (No. GUTQDJJ2017002).

References

[1] K.C. Lai, L.Y. Lee, B.Y.Z. Hiew, S. Thangalazhy-Gopakumar, S. Gan, Environmental application of three-dimensional graphene materials as adsorbents for dyes and heavy metals: review on ice-templating method and adsorption mechanisms, J. Environ. Sci., 79 (2019) 174–199.
[2] A.A. Siyal, M.R. Shamsuddin, M.I. Khan, N.E. Rabat, M. Zulfiqar, Z. Man, J. Siame, K.A. Azizli, A review on geopolymers as emerging materials for the adsorption of heavy metals and dyes, J. Environ. Manage., 224 (2018) 327–339.
[3] V.K. Gupta, Dr. Suhas, Application of low-cost adsorbents for dye removal–a review, J. Environ. Manage., 90 (2009) 2313–2342.
[4] N.P. Raval, P.U. Shah, N.K. Shah, Adsorptive amputation of hazardous azo dye Congo red from wastewater: a critical review, Environ. Sci. Pollut. Res., 23 (2016) 14810–14853.
[5] S. Cheng, L. Zhang, A. Ma, H.Y. Xia, J.H. Peng, C.Y. Li, J.H. Shu, Comparison of activated carbon and iron/cerium modified activated carbon to remove methylene blue from wastewater, J. Environ. Sci., 65 (2018) 92–102.
[6] C. Yin, C. Xu, W.H. Yu, Y.X. Jia, W.Z. Sun, G.Z. Zhou, M. Xian, Synthesis of a novel isatin and ethylenediamine modified resin and effective adsorption behavior towards Orange G, RSC Adv., 9 (2019) 801–809.
[7] N.P. Raval, P.U. Shah, N.K. Shah, Nanoparticles loaded biopolymer as effective adsorbent for adsorptive removal of malachite green from aqueous solution, Water Conserv. Sci. Eng., 1 (2016) 69–81.
[8] N.P. Raval, P.U. Shah, D.G. Ladha, P.M. Wadhwani, N.K. Shah, Comparative study of chitin and chitosan beads for the adsorption of hazardous anionic azo dye Congo red from wastewater, Desal. Water Treat., 57 (2016) 9247–9262.
[9] M. Cheng, G.M. Zeng, D.L. Huang, C. Lai, P. Xu, C. Zhang, Y. Liu, Hydroxyl radicals based advanced oxidation processes (AOPs) for remediation of soils contaminated with organic compounds: a review, Chem. Eng. J., 284 (2016) 582–598.
[10] N.P. Raval, P.U. Shah, N.K. Shah, Malachite green "a cationic dye" and its removal from aqueous solution by adsorption, Appl. Water Sci., 7 (2017) 3407–3445.
[11] Q. Liu, Y. Gao, Y. Zhou, N. Tian, G.F. Liang, N. Ma, W. Dai, Highly improved water resistance and Congo red uptake capacity with a Zn/Cu-BTC@MC composite adsorbent, J. Chem. Eng. Data, 64 (2019) 3323–3330.
[12] R. Gong, Y. Jin, J. Chen, Y. Hu, J. Sun, Removal of basic dyes from aqueous solution by sorption on phosphoric acid modified rice straw, Dyes Pigm., 73 (2007) 332–337.
[13] L.S. Oliveira, A.S. Franca, T.M. Alves, S.D.F. Rocha, Evaluation of untreated coffee husks as potential biosorbents for treatment of dye contaminated waters, J. Hazard. Mater., 155 (2008) 507–512.
[14] N.P. Raval, P.U. Shah, D.G. Ladha, M.K. Vekariya, P.M. Wadhwani, N.K. Shah, Synthesis, characterization and adsorption significance of novel composite (chitosan beads loaded nickel-oxide nanoparticles), Desal. Water Treat., 62 (2017) 387–402.
[15] L. Zang, X. Qiao, L. Hu, C. Yang, Q. Liu, C. Wei, J.H. Qiu, H.D. Mo, G. Song, J. Yang, C.J. Liu, Preparation and evaluation of coal fly ash/chitosan composites as magnetic supports for highly efficient cellulose immobilization and cellulose bioconversion, Polymers, 10 (2018) 523.
[16] Z.S. Chen, J. Wang, Z.X. Pu, Y.S. Zhao, D.H. Jia, H.X. Chen, T. Wen, B. Hu, A. Alsaedi, T. Hayat, X. Wang, Synthesis of magnetic Fe_3O_4/CFA composites for the efficient removal of U(VI) from wastewater, Chem. Eng. J., 320 (2017) 448–457.
[17] K.O. Santos, R.C. Barbosa, J.S. Buriti, A.G.B. Junior, W.J.B. Sousa, S.M.C. Barros, R.J. Oliveira, M.V.L. Fook, Thermal, chemical, biological and mechanical properties of chitosan films with powder of eggshell membrane for biomedical applications, J. Therm. Anal., 136 (2019) 725–735.
[18] J.Z. Wang, G.H. Zhao, Y.F. Li, X. Liu, P.P. Hou, Reversible immobilization of glucoamylase onto magnetic chitosan nanocarriers, Appl. Microbiol. Biotechnol., 97 (2013) 681–692.
[19] R. Gong, J.J. Ye, W. Dai, X.Y. Yan, J. Hu, X. Hu, S. Li, H. Huang, Adsorptive removal of Methyl orange and Methylene blue from aqueous solution with finger-citron-residue-based activated carbon, Ind. Eng. Chem. Res., 52 (2013) 14297–14303.
[20] W. Dai, Y.C. Liu, W. Su, G.S. Hu, G. Deng, X. Hu, Preparation and CO_2 sorption of high surface area activated carbon from KOH activation of finger citron residue, Adsorpt. Sci. Technol., 30 (2012) 183–191.
[21] W.L. Xie, J.L. Wang, Immobilized lipase on magnetic chitosan microspheres for transesterification of soybean oil, Biomass Bioenergy, 36 (2012) 373–380.
[22] G.K. Sarma, S. SenGupta, K.G. Bhattacharyya, Adsorption of monoazo dyes (Crocein orange G and Procion red MX5B) from water using raw and acid-treated montmorillonite K10: insight into kinetics, isotherm, and thermodynamic parameters, Water Air Soil Pollut., 229 (2018) 312.
[23] A. Ornek, M. Ozacar, I.A. Sengil, Adsorption of lead onto formaldehyde or sulphuric acid treated acorn waste: equilibrium and kinetic studies, Biochem. Eng. J., 37 (2007) 192–200.
[24] H.L. Zang, Y.-H. Li, Y. Li, L. Chen, Q.J. Du, K.X. Zhou, H. Li, Y. Wang, L. Ci, Adsorptive removal of cationic dye from aqueous solution by graphene oxide/cellulose acetate composite, J. Nanosci. Nanotechnol., 19 (2019) 4535–4542.
[25] R. Zhang, J. Zhang, X. Zhang, C.C. Dou, R. Han, Adsorption of Congo red from aqueous solutions using cationic surfactant modified wheat straw in batch mode: kinetic and equilibrium study, J. Taiwan Inst. Chem. Eng., 45 (2014) 2578–2583.
[26] H. You, J.C. Chen, C. Yang, L. Xu, Selective removal of cationic dye from aqueous solution by low-cost adsorbent using phytic acid modified wheat straw, Colloid Surf., A, 509 (2016) 91–98.
[27] E. Daneshvar, A. Vazirzadeh, A. Niazi, M. Kousha, Mu. Naushad, A. Bhatnagar, Desorption of Methylene blue dye from brown macroalga: effects of operating parameters, isotherm study and kinetic modeling, J. Cleaner Prod., 152 (2017) 443–453.
[28] B. Samiey, S. Golestan, Adsorption of Triton X-100 on silica gel: effects of temperature and alcohols, Cent. Eur. J. Chem., 8 (2010) 361–369.
[29] M. Rafi, B. Samiey, C.-H. Cheng, Study of adsorption mechanism of Congo red on graphene oxide/PAMAM nanocomposite, Materials, 11 (2018) 496.
[30] B. Samiey, F. Ashoori, Adsorptive removal of Methylene blue by agar: effects of NaCl and ethanol, Chem. Cent. J., 6 (2012) 14.
[31] N.S. Beyranvand, B. Samiey, A.D. Tehrani, Adsorption mechanism of Congo red on Mg-Al-layered double hydroxide nanocompound, Acta Chim. Slov., 66 (2019) 443–454.
[32] X.C. Lai, G.X. Luo, Synthesis of mesoporous α-MnO_2 in manganese(II)-based deep eutectic solvent and their application in the absorption of Congo red, Sep. Sci. Technol., 54 (2019) 1269–1277.
[33] K. Durairaj, P. Senthilkumar, P. Velmurugan, S. Divyabharathi, D. Kavitha, Development of activated carbon from *Nerium oleander* flower and their rapid adsorption of direct and reactive dyes, Int. J. Green Energy, 16 (2019) 573–582.
[34] F. Kallel, F. Chaari, F. Bouaziz, F. Bettaieb, R. Ghorbel, S.E. Chaabouni, Sorption and desorption characteristics for the removal of a toxic dye, methylene blue from aqueous solution by a low cost agricultural by-product, J. Mol. Liq., 219 (2016) 279–288.
[35] P.K. Neghlani, M. Rafizadeh, F.A. Taromi, Preparation of aminated-polyacrylonitrile nanofiber membranes for the adsorption of metal ions: comparison with microfibers, J. Hazard. Mater., 186 (2011) 182–189.
[36] C.X. Zhu, Y.X. Xia, Y.Y. Zai, Y.Q. Dai, X.Y. Liu, J. Bian, Y. Liu, J.S. Liu, G. Li, Adsorption and desorption behaviors of HPEI and thermoresponsive HPEI based gels on anionic and cationic dyes, Chem. Eng. J., 369 (2019) 863–873.